International Transactions on Electrical Engineering and Computer Science
K Y Jo et.al., Vol: 5, No: 1, pp: 17-34, March 2026

# Simulation and Dynamic Analysis of BLDC Motor Speed Control in Four Quadrants across Diverse Operating Conditions

Kun-Yik Jo[1], Hyunho Park

**Abstract:** This article presents a comprehensive analysis and simulation of a Brushless DC (BLDC) motor drive system, emphasizing its performance in four-quadrant operations under various operating conditions. The proposed model leverages MATLAB/Simulink and integrates closed loop proportional integral (PI) control with hysteresis current regulation to enhance speed and torque stability. The study demonstrates the model's capability to achieve robust performance, rapid transient response, and efficient energy utilization, including regenerative braking. Comparative evaluations highlight the effectiveness of the proposed control scheme over traditional and advanced methodologies such as fuzzy logic and ANFIS based systems. The findings underscore the system's adaptability to nonlinearities and load disturbances, making it an optimal solution for industrial and electric vehicle applications. Future work suggests exploring AI-based adaptive control to further optimize performance.

**Keywords:** BLDC Motor, Speed control, Power quality, Chopper.

## 1. Introduction

Due to their efficiency, quietness, compactness, reliability, and minimal maintenance requirements, Brush less DC (BLDC) motors are the optimal choice for control applications that require modest horsepower. These motors have been difficult to use for variable speed applications over time. The production of PM brushless electric motors, control schemes, microprocessors, drivers with speed adjustment, and power semiconductor technology has advanced, resulting in cost effective and dependable solutions for adjustable speed applications [1].

**History**
Received: 10-12-2025; Revised: 30-01-2026;
Accepted: 01-03-2026

✉ Kun-Yik Jo
jky0451@naver.com

[1]Department of Electrical Engineering, Chonnam National University, Gwangju – 61186, South Korea.

In the domestic appliance sector, electronic motor drivers will experience a surge in popularity over the next five years. Universal motors and 1-Φ AC Induction Motors (IM) have been employed in a variety of appliances, such as washing machines, AC, refrigerators, vacuum cleaners, and freezers. Older systems use main AC electricity at a fixed speed without considering efficiency [2-5]. Traditional motors cannot match consumer demands for lower energy use, higher performance, decreased noise, and increased convenience. Permanent Magnet Synchronous Machines (PMSM) and BDCMs may be viable alternatives to induction motors in servo applications, according to recent studies [6]. Both the BDCM and the PMSM employ rectangular stator currents and back EMFs to maintain a constant torque, but the PMSM employs sinusoidal currents and back EMFs. Both industry and academia are confused about motor type models. PMSMs are synchronous machines with a wound rotor that do not have damper windings. They utilize permanent magnets for excitation, rather than field windings [7-10].

The d-q PMSM model can be derived from the famous synchronous machine model by removing the

https://doi.org/10.62760/iteecs.5.1.2026.176

equations for damper windings and field current dynamics. Because the inductances would fluctuate due to the non-sinusoidal nature of the back EMF, the BDCM would not gain any benefit from transforming the equations to the d-q frame. Rather, the BDCM's ABC phase variable model is recommended since it allows for a more comprehensive analysis of the motor's torque behaviour [11]. We have studied the high-performance vector-operated PMSM servo drives' transient behaviour using the d-q PMMS model, and we have studied the behaviour of BDCM speed servo drives using the ABC phase variable model. Prior research has examined the application properties of both motor types [12-14]. Presenting both models together, this paper demonstrates that the abc model is more suited for researching BDCMs, while the d-q model is better suited for in-depth investigation of PMSMs. A BLDCM servo system's design usually entails a laborious trial-and-error procedure that frequently falls short of performance optimization. Modelling, developing a control scheme, simulating, and fine-tuning parameters are all part of the intricate process of building a BLDCM drive [15-17]. A PI controller is often recommended for BLDCM control due to its effectiveness in linear motor control. Nevertheless, the driver and load introduce non-linear elements in many real-world applications, which reduces the PI controller's effectiveness for non-linear systems. Permanent magnet motors require an appropriate speed controller to operate at their best. A PI controller is typically used to implement speed control. Despite being widely employed in industry because of their straightforward design and simplicity of use, PI controllers struggle to handle complicated control problems including parametric fluctuations, load disturbances, and nonlinearity. Additionally, the nonlinear models of PMBLDC motors are not appropriate for PI controllers, which need exact linear mathematical models [18-22].

The motor drive system's dynamic behaviour is improved and its resistance to load disturbances and parameter changes is increased when fuzzy logic (FL) control is used for speed regulation. Unlike conventional controllers, fuzzy logic control is naturally resilient to variations in load and provides increases in speed reaction quality. Fuzzy logic controllers are also a more flexible option for controlling BLDC motors because they are simple to install and do not require exact mathematical models.

The other paper is organized in various sections. Section 2 presents the literature, Section 3 about BLDC drive test system, Section 4 about modelling, Results in Section 5 and Section 6 conclusions.

## 2. Literature Survey

Under optimal circumstances, the torque produced by brushless DC motors stays constant. However, one of the biggest challenges facing the automotive industry is regulating fast-moving vehicles using BLDC motors. This study uses a BLDC drive and suggests a Multi Level Inverter (MLI) layout that uses fewer switches. Improving the performance of BLDC drives compared to typical inverters is the goal of this effort, which employs multiple inverters. Furthermore, using creative alterations in the suggested MLI topology, the study investigates current electrical braking techniques applied to the BLDC motor [1]. This paper introduces a PID controller and an ANNC for controlling the BLDC motor’s speed. The BLDC motor's response is enhanced by the Artificial Neural Networks (ANN), leading to more consistency and reliability. It reduces peak, overrun, and settling times while increasing the system's reaction speed [2]. Here we also have a look at how a PMBLDC motor can run without a position sensor. Using a hybrid technique, the ZCP of the Back EMFs is found from the terminal voltages. One component of the proposed hybrid model is a Particle Swarm Optimization (PSO) trained controller for the Adaptive Neuro Fuzzy Inference System (ANFIS). A ZCP detecting circuit receives its estimated sample signals from the ANFIS controller, which processes line voltages as inputs. By modifying the ANFIS parameters and creating the right commutation control for the inverter, this system leverages PSO to reduce errors between the estimated and actual outputs [3]. Worldwide, more and more people are looking for alternatives to oil-powered vehicles, and electric vehicles (EVs), which can be two- or four-wheelers, are becoming more popular. The advantages of BLDC motors make them ideal for use in traction and industrial settings. Smooth acceleration of EV depends on low inaccuracy in both steady-state and transient reactions. This work showcases the construction and functioning of a BLDC motor for

controlling speed during acceleration and deceleration, with a focus on minimising errors within the MATLAB/Simulink environment. Motor control performance is often improved with the use of fuzzy and PI controllers. This study examines the ANFIS and PI controllers in relation to a 5 kW, 48 V, 100-Amp BLDC motor used in electric vehicle settings [4]. The superior torque, efficiency, and speed control over traditional motors, BLDC motors are becoming more and more common in robots, electric vehicles, and other industrial applications. Enhancing the total loss, volume, and cost-effectiveness of BLDC motors is the goal of this work, which employs optimisation approaches grounded in collective intelligence. Structure of the BLDC motor is optimized utilizing a range of optimization approaches. Through these optimization techniques, the study offers insights into the rates of convergence and ideal design parameters, and the standard deviation is used to evaluate each method's stability [5].

This study presents the utilization of a controller for BLDC motor drives that is built on fuzzy logic. The rules of the fuzzy system are constructed using the Lyapunov function in the initial stage of the project, which involves developing the fuzzy model. The Chameleon Swarm Algorithm (CSA) is used to optimize the controller's gain coefficients. Simulation tests examine a number of variables, such as optimization phases, the effect of controller parameters on control precision, and resilience against parameter changes. According to the results, even when there are changes in the motor's mechanical time constants or other parameters, the fuzzy speed controller maintains high precision and steady operation [6]. Implant treatments are the main application for BLDC micro-motors in the field of dental prosthesis. The requirement for motors that can precisely process dental materials is increasing as these materials get harder. However, maintaining price competitiveness is difficult due to the high cost of sophisticated motors. For accurate machining of hard dental materials, dental motors need to be able to drill at low speeds with high torque and rotate at high speeds. They also need to be able to control heat to prevent burns to users. High-resolution position sensors, like encoders, are often used in motors that need precise control. However, they are expensive and take up a lot of space, which could make them less competitive. This study presents a way for controlling a BLDC micro-motor that uses an inexpensive Hall sensor often used in the dental industry. It is capable of precision milling at low speeds, high torque, and high speeds without modifying the hardware [7]. Consumer appliances frequently employ low-power BLDC motors. Although precise speed regulation is still required, these motors' frequently high winding resistance can do away with the necessity for current control loops. To minimize noise and harmonics, this study investigates the use of improved sinusoidal PWM. The third harmonic component is added to sine wave transmission method to lower torque ripple. A fuzzy logic block should also be added to the usual PID speed driver, according to the study. According to simulation results, using the fuzzy-based PID controller instead of the conventional PID controller decreases overshoot and cuts transient time from 0.2 to 0.05 seconds [8].

This work introduces the TID controller technique to enhance BLDC motor speed control, which is very useful in electric vehicle applications. To guarantee accurate and effective functioning, the TID controller regulates the motor's torque, speed, and position. PID and PI controllers' performance is contrasted with that of TID controllers. TID control is the best option for effective and responsive BLDC drive applications since it enhances torque and current stability, transient responsiveness, and robustness to disturbances, according to results [9].

The problems of overshoot, quick response, and inadequate anti-disturbance in BLDC motor control are addressed in this work. We compare PI control to a six-step commutation control method that is based on second order Active Disturbance Rejection Control (ADRC). Both the PI and ADRC control approaches can follow target signals without overshooting, as shown in simulations and real world tests with the STM32F4 controller. The ADRC approach is a very successful control strategy because it offers excellent robustness at different operating speeds and great anti-load disturbance capabilities [10].

BLDC motors undergo changes in current waveforms at high speeds, which raise torque ripple and restrict motoring torque. This problem occurs because the motor's EMF prevents the phase current from reaching the intended value. To fix this, the

phase turn-on angle is advanced so that commutation starts earlier. Since BLDC motors might fluctuate in speed, the turn-on angle should advance automatically in response to the motor's speed. In this paper, we provide a microcontroller-based autonomous real-time electronic governor that can achieve the desired profile of speed, torque, and advancement angle [11]. The control procedure for BLDC motors is simplified while rotor phase position and speed estimates are enhanced through the implementation of ANN control technique that is based on a MLP architecture. By conditioning the motor's phase voltage, we may provide the MLP approach with inputs that have a high signal-to-noise ratio. The network learns from the encoder signal and uses the rotor's voltage and position characteristics to make speed and position estimations. The motor control system incorporates this method after training and discretization [12].

A PWM-PWM logic is used to decrease torque ripple while keeping steady-state performance and rapid dynamic response. A novel PWM technique and an advanced angle approach are provided by this technology to reduce torque ripple in a PMBLDC motor drive. By reducing the phase voltage and current displacement, the suggested angle method improves torque production [13]. More and more applications are utilizing BLDC motor drives due to its increased power density and efficiency. All four-quadrant operations of a three phase BLDC motor are investigated in this paper using conventional control. The technology uses regenerative braking to save energy and runs without losing power. In order to save system costs, the controller makes use of a Digital Signal Processor (DSP), which provides increased speed, resolution, and algorithm implementation capabilities [14]. A fuzzy logic controller that can control the speed of BLDC motors in both directions which are utilized in four-quadrant operations without power loss is presented in this study. A bidirectional DC-DC converter stores extra energy in the battery during regenerative braking. By charging and discharging the battery in response to motor speed and braking circumstances, this technology offers effective energy management [15]. A BLDC motor's position can be controlled using a unique hybrid control technique that combines model-free adaptive control (MFAC) and discrete-time sliding mode control (SMC). The data-driven control approach is appropriate for real-time platforms such as gimbal systems since it reduces simulation time and complexity. This method improves control and streamlines implementation because it doesn't require a system model [16]. With an emphasis on minimizing torque ripple, this work develops a simulation model for BLDC motor operation in all four quadrants. In order to ensure effective functioning during regenerative braking, a Model Predictive Controller (MPC) regulates the motor's speed, torque, and energy conservation [17].

As a means of rapid control prototyping for closed-loop speed control, this study examines a BLDC motor drive arrangement with a dSPACE DS1103 controller board. The real-time performance of the drive is heavily influenced by elements such as the execution of real-time control software, speed and position measurements, data collecting, and more. Despite this, control methods for motor drives typically produce good simulation results under steady-state and transient settings. This is case despite the fact that the drive's performance is largely dependent on these elements. Hardware implementation presents a number of obstacles, the most significant of which are selecting the appropriate hardware and correctly configuring it with the controller board [18].

Using a bi-directional DC-DC converter to drive a BLDC motor in all four directions (forward, reverse driving, stopping, and reversing) is the focus of this research project. A 3-Φ Voltage Source Inverter (VSI) takes input from the DC-DC converter and uses it to power the motor. During regenerative mode, the vehicle converts mechanical energy into electrical energy through boost operation. This converted energy is then stored in the same battery. While the car is moving, though, the bi-directional converter puts the battery into buck mode. The technique uses regenerative braking to collect energy during each stop because EVs stop and start a lot. Furthermore, regulated speed regulation enables energy return to the battery when the EV is descending [19].

Photovoltaic (PV) water pumping systems are rapidly gaining popularity, especially in renewable energy applications. This study zeroes in on a specific system where the converter is vital for effectively

extracting electricity from the PV array. The suggested setup makes use of an M-LUO converter, which is a DC-based intermediate DC-DC power converter, to maximise the amount of power that can be harvested. The M-LUO converter is managed using an MPPT approach based on Grey Wolf Optimization (GWO). This technique helps to ensure that a BLDC motor starts up without any friction. By reaching the VSI's fundamental switching frequency in the BLDC motor, electronic commutation avoids losses often caused by high switching frequencies. This paper compares the GWO-optimized algorithm to several other Maximum Power Point Tracking (MPPT) methods, such as Perturb and Observe (P&O) and fuzzy logic-based approaches. By comparing the rotor's position to the reference speed, a PI controller regulates the speed of a BLDC motor. Not only that, but this study details how to build a BLDC-based pumping motor with an optimized high-gain boost converter using the GWO method [20]. Instead of employing traditional back-to-back converters, this study suggests using a single-stage DMC to regulate the speed of a BLDC motor while maintaining its power quality constant. The most significant benefit of utilizing DMC is that it lessens the amount of losses that occur at the converter stage. The converter stage of a back-to-back converter uses nine switches instead of twelve. The system's resilience is further increased by eliminating the large DC-link storage capacitor, which gives the motor controller a completely silicon-based solution. To top it all off, the matrix converter's indirect modulation method enables closed-loop hysteresis current regulation on the load side, which ensures precise control of the motor speed. On the grid side, the utilization of Space Vector Modulation (SVM) leads to an improvement in the input power factor with minimal distortion [21]. Industrial and non-industrial applications make extensive use of BLDC motors. One of the main objectives for producers and researchers is to lower the cost and boost the dependability of these motors. By limiting the requirement for current or voltage sensors, removing position sensors, and reducing the number of switches, a significant improvement has been accomplished. Electrolytic capacitors, which are expensive and prone to failure, continue to be a significant obstacle, nonetheless. This study's overarching goal is to suggest a novel control system capable of controlling both speed and torque in tandem. Using low-capacity thin-film capacitors in the DC link instead of high-capacity electrolytic capacitors is the primary objective of this research. By using this method, torque ripples brought on by variations in the DC link's voltage are lessened [22]. PMBLDC motors offer numerous advantages over conventional machines, such as high efficiency and variable speed controllability. For domestic applications, where cost-effectiveness is crucial, simplicity is crucial, even though there are numerous prototypes with intricate designs that guarantee excellent efficiency.

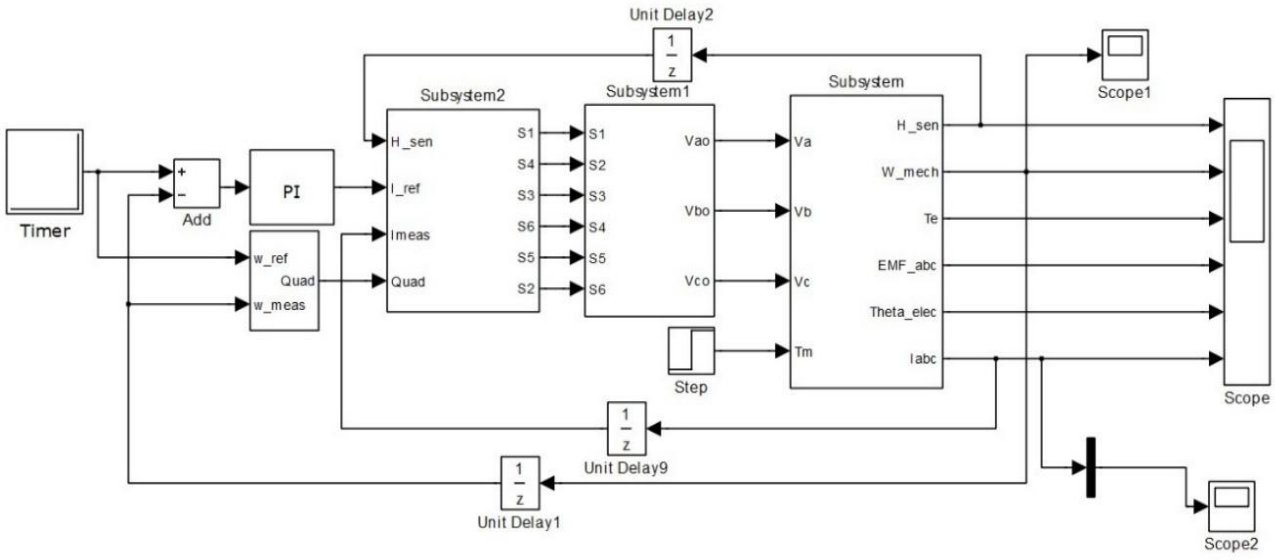


**Fig. 1:** Simulink model of BLDC drive system

A comparison of several computer models for a tiny PM BLDC motor with a single ferrite magnet rotor is shown in this article. The FEM is engaged to compare several design solutions for basic PM BLDC actuators, with an emphasis on those appropriate for home appliances [23].

## 3. Description and modelling of the drive system

Fig. 1, shows the primary components of the driving system. The four quadrant operating BLDC motor, inverter, current controller, speed controller, and quadrant determination block are all part of this. The system is built by combining each of these pieces, which are first modelled independently.

### *3.1 Modelling of BLDC motor*

As illustrated in Fig. 2, a three-phase inverter must be installed at the front of an electronic motor. The inverter acts as an electrical commutator when operating in self-control mode, receiving switching logic pulses from the absolute position sensors. An electrically commutated motor is another term for this type of drive. There are two main modes of operation for the inverter:

- 2π/3 angle switch on mode.
- PWM mode with voltage and current control.

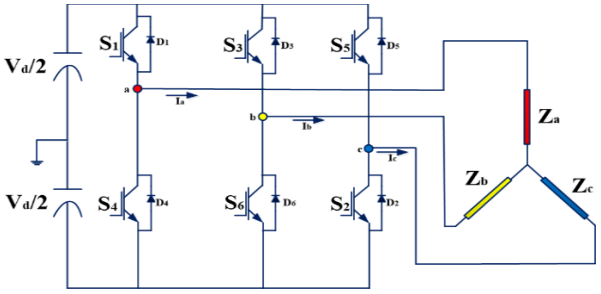


**Fig. 2:** On mode for the 2π/3 angle switch

The inverter waveform for this mode is displayed in Fig. 3. At the centre of each phase voltage wave across the *2π/3* angle, the six switches of the inverter, $T_1$-$T_6$, symmetrically place the input DC current, $I_d$. While $\alpha$ is zero, the waves of current and voltage are in perfect harmony. The angle $\alpha$ indicates how far ahead the current wave is in relation to the voltage wave. There are two switches that are always turned on: one from the lower group and one from the upper group. Take time $t_1$, for example. With switches $T_1$ and $T_6$ open, the supply voltage $V_{dc}$ and current $I_d$ are across the line that connects phases A and B. This setup has $I_d$ being negative in phase B and positive in phase A. At the halfway of phase A, $T_2$ is activated, and $T_6$ is deactivated, while $T_1$ continues conduction along the entire *2π/3* angle. Consequently, $I_d$ is transferred from phase B to phase C due to this switching, although it remains in phase A. Throughout the entire cycle, the conduction pattern indicates switching modes by changing every *π/3* angle. The precise timing of device switching or commutation during the wave is determined by the absolute position sensor. As a result, the inverter basically serves as an electronic commutator that is sensitive to the location of the rotor.

### *3.2 PWM mode with voltage and current control*

The inverter switches were programmed to act as a commutator in the previous mode, turning the devices on and off in succession for a time of *2π/3*. Along with their commutator function, the switches can also be operated in PWM chopping mode to continuously alter the voltage and current at the machine terminals. The two primary chopping modes for the inverter's current-controlled functioning are FB mode and FW mode. In both modes, the machine's average voltage VAV and average current IAV can be adjusted, as the devices are powered on and off in response to the duty cycle.

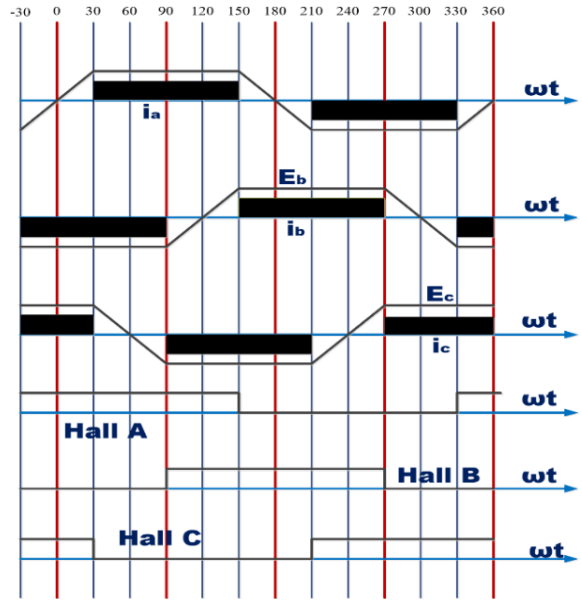


**Fig. 3:** Hall position sensors, current waveforms, and back-emfs for BLDC

### *3.3 Position Sensors of Rotors*

A reliable source of information for coordinating motor excitation with rotor position it is shown in Fig. 4, Hall Effect sensors ensure constant torque production. To detect changes in the magnetic field, these sensors use Hall sensors that are activated by rotor magnets. The Hall switch and signal conditioning circuit work together to generate pulses with sharp edges that are compatible with TTL. There are three Hall sensors on the stator frame, and they are spaced $120^0$ apart. The rotor's location is precisely sensed using the digital data from the Hall sensors.

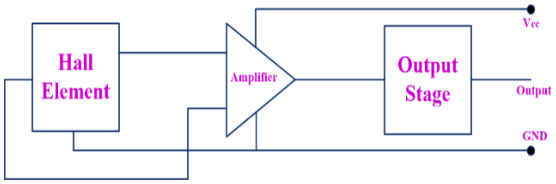


**Fig. 4:** Hall position sensors

### *3.4 Mathematical Modelling*

Three windings on the stator and a rotor with a permanent magnet are characteristics of the BLDCM. Rotor induced currents are not significant in materials with high resistivity, such as magnets and stainless steel. Without considering the damper windings in the model, the three-winding circuit equation in phase variables can be found as in equation (1).

$$\begin{bmatrix} v_{as} \\ v_{bs} \\ v_{cs} \end{bmatrix} = \begin{bmatrix} R_s & 0 & 0 \\ 0 & R_s & 0 \\ 0 & 0 & R_s \end{bmatrix} \begin{bmatrix} i_a \\ i_b \\ i_c \end{bmatrix} + \frac{d}{dt} \begin{bmatrix} L_{aa} & L_{ab} & L_{ac} \\ L_{ba} & L_{bb} & L_{bc} \\ L_{ca} & L_{cb} & L_{cc} \end{bmatrix} \begin{bmatrix} i_a \\ i_b \\ i_c \end{bmatrix} + \begin{bmatrix} e_a \\ e_b \\ e_c \end{bmatrix} \quad (1)$$

Where $v_{as}, v_{bs}$ *and* $v_{cs}$ are the stator phase voltages $R_s$ is the stator resistance per phase $i_a, i_b$ *and* $i_c$ are the stator phase currents $L_{aa}, L_{bb}$ *and* $L_{cc}$ are the self-inductance of phases a, b and c $L_{ab}, L_{bc}$ *and* $L_{ac}$ are the mutual inductances between phases a, b and c $e_a, e_b$ *and* $e_c$ are the phase back electromotive forces. It has been assumed that the resistance of all the windings is equal. It has also been assumed that if there is no change in the rotor reluctance with angle because of a non-salient rotor and then (2) and (3), as

$$L_{aa} = L_{bb} = L_{cc} = L \quad (2)$$

$$L_{ab} = L_{ba} = L_{ac} = L_{ca} = L_{bc} = L_{cb} = M \quad (3)$$

Equations (2) and (3) can be substituted in (1) to obtain the model as (4)

$$\begin{bmatrix} v_{as} \\ v_{bs} \\ v_{cs} \end{bmatrix} = \begin{bmatrix} R_s & 0 & 0 \\ 0 & R_s & 0 \\ 0 & 0 & R_s \end{bmatrix} \begin{bmatrix} i_a \\ i_b \\ i_c \end{bmatrix} + \frac{d}{dt} \begin{bmatrix} L & M & M \\ M & L & M \\ M & M & L \end{bmatrix} \begin{bmatrix} i_a \\ i_b \\ i_c \end{bmatrix} + \begin{bmatrix} e_a \\ e_b \\ e_c \end{bmatrix} \quad (4)$$

Where $v_{as}, v_{bs}$ *and* $v_{cs}$ are the stator phase voltages, may be designed as (5),

$$v_{as} = v_{a0} - v_{n0}, v_{bs} = v_{b0} - v_{n0} \text{ and } v_{cs} = v_{c0} - v_{n0} \quad (5)$$

Where the neutral and three-phase voltages, $V_{a0}, V_{b0}, V_{c0}$ *and* $V_{n0}$ are referred to the zero reference potential at the midpoint of the DC connection.
It is required that the stator phase currents be balanced, as presented in equation (6)

$$i_a + i_b + i_c = 0 \quad (6)$$

As a result, the inductances matrix in the models becomes simpler, as equation (7)

$$Mi_b + Mi_c = -Mi_a \quad (7)$$

Therefore, in state space from, the equation (8) gives,

$$\begin{bmatrix} v_{as} \\ v_{bs} \\ v_{cs} \end{bmatrix} = \begin{bmatrix} R_s & 0 & 0 \\ 0 & R_s & 0 \\ 0 & 0 & R_s \end{bmatrix} \begin{bmatrix} i_a \\ i_b \\ i_c \end{bmatrix} + \frac{d}{dt} \begin{bmatrix} L-M & 0 & 0 \\ 0 & L-M & 0 \\ 0 & 0 & L-M \end{bmatrix} \begin{bmatrix} i_a \\ i_b \\ i_c \end{bmatrix} + \begin{bmatrix} e_a \\ e_b \\ e_c \end{bmatrix} \quad (8)$$

It has been assuming that back EMF $e_a, e_b$ *and* $e_c$ have trapezoidal wave from (9)

$$\begin{bmatrix} e_a \\ e_b \\ e_c \end{bmatrix} = \omega_m \lambda_m \begin{bmatrix} f_{as}(\theta_r) \\ f_{bs}(\theta_r) \\ f_{cs}(\theta_r) \end{bmatrix} \quad (9)$$

Where $\omega_m$ is the angular rotor speed in radians per second. $\lambda_m$ is the flux linkage. With a maximum of ±1, the functions $f_{as}(\theta_r), f_{bs}(\theta_r)$ *and* $f_{cs}(\theta_r)$ are similar in shape to , $e_b$ *and* $e_c$. Rotor locations are represented by $\theta_r$ in radians. The sharp corners are absent from the induced emfs because of their trapezoidal shape. The electromagnetic fields are generated by the flow linkages' derivatives, which are functions that are continuous. Fringing smooths out the flux density

curve as well, removing any sharp edges. According to Newton's definition, the electromagnetic torque is (10),

$$T_e = \frac{[e_a i_a + e_b i_b + e_c i_c]}{\omega_m} \ (N-m) \quad (10)$$

The armature voltage and phase voltage calculations for a DC machine are the same. For this and other reasons, this apparatus is known as the BLDC machine. The moment of inertia is defined as (11)

$$J = J_m + J_l \quad (11)$$

With load torque $T_l$, friction coefficient $B$, and inertia $J$, the equation for the simple motion system is (12)

$$J\frac{d\omega_m}{dt} + B\omega_m = (T_e - T_l) \quad (12)$$

The electrical rotor speed and position are (13)

$$\frac{d\theta_r}{dt} = \frac{p}{2}\omega_m \quad (13)$$

It is common practice to disregard the system when the damping coefficient $B$ is small. Rotor position $\theta_r$ is represented by the equation above, which repeats every 2π. To prevent applied voltage imbalance and model drive performance, the neutral point's potential in relation to the zero potential $V_{n0}$ must be considered. Equation (6) is substituted into the volt-ampere equation (8) to yield this, which is then added to give (14),

$$v_{a0} + v_{b0} + v_{c0} - 3v_{n0} = R_s(i_a + i_b + i_c) + (L-M)(pi_a + pi_b + pi_c) + (e_a + e_b + e_c) \quad (14)$$

When we replace equation (6) with equation (14) we obtain (15)

$$v_{a0} + v_{b0} + v_{c0} - 3v_{n0} = (e_a + e_b + e_c) \text{ thus}$$

$$v_{n0} = \frac{[(v_{a0} + v_{b0} + v_{c0}) - ((e_a + e_b + e_c))]}{3} \quad (15)$$

The variables $i_a, i_b, i_c, \omega_m$ *and* $\theta_r$ time are regarded as independent variables in the model that is produced. When all pertinent equations are combined, the system in state-space form is equation (16),

$$x = Ax + Bu + Ce \quad (16)$$

Where, $x = [i_a \quad i_b \quad i_c \quad \omega_m \quad \theta_r]^t$

$$A = \begin{bmatrix} -\frac{R_s}{L-M} & 0 & 0 & -\frac{\lambda_m}{J}f_{as}(\theta_r) & 0 \\ 0 & -\frac{R_s}{L-M} & 0 & -\frac{\lambda_m}{J}f_{bs}(\theta_r) & 0 \\ 0 & 0 & -\frac{R_s}{L-M} & -\frac{\lambda_m}{J}f_{cs}(\theta_r) & 0 \\ \frac{\lambda_m}{J}f_{as}(\theta_r) & \frac{\lambda_m}{J}f_{bs}(\theta_r) & \frac{\lambda_m}{J}f_{cs}(\theta_r) & -\frac{B}{J} & 0 \\ 0 & 0 & 0 & \frac{P}{2} & 0 \end{bmatrix}$$

$$B = \begin{bmatrix} \frac{1}{L-M} & 0 & 0 & 0 \\ 0 & \frac{1}{L-M} & 0 & 0 \\ 0 & 0 & \frac{1}{L-M} & 0 \\ 0 & 0 & 0 & \frac{1}{L-M} \end{bmatrix}$$

$$C = \begin{bmatrix} -\frac{1}{L-M} & 0 & 0 \\ 0 & -\frac{1}{L-M} & 0 \\ 0 & 0 & -\frac{1}{L-M} \end{bmatrix}$$

$$u = [v_{as} \quad v_{bs} \quad v_{cs} \quad T_l]^t$$

$$e = [[e_a \quad e_b \quad e_c]^t]$$

## 4. Modelling the BLDC motor drive system's speed control

A current controller that uses PWM, a Reference Current Generator (RCG), a PMBLDC motor, an IGBT inverter, and a PI speed controller are all components of the drive system under discussion. To enable real-time simulation, we have modelled and combined all these components.

### *4.1 Reference Current Generator*

By applying the reference torque $T_{ref}$, we may find the magnitude of the three-phase current $i_{ref}$, as (17),

$$i_{ref} = \frac{T_{ref}}{Kt} \quad (17)$$

Where $K_t$ is the torque constant expression. A three phase reference current $(i_a^*, i_b^*, i_c^*)$ is generated by the reference current generator block based on the reference current magnitude value $i_{ref}$ and the rotor position. It is possible to input reference currents into the PWM current controller. Based on the rotor's position, the reference currents of each phase $i_a^*, i_b^*, i_c^* f$ are determined. The reference currents,

rotor position signal, and currents are indicated in Table. 1, are all inputted into the PWM current controller, Table. 2, illustrates the reference currents for forward motoring and reverse braking mode of operation and Table. 3, illustrates the reference currents for reverse motoring and forward braking and the mode of operations.

**Table. 1:** Currents for reference and rotor position signals

| Rotor Position $\theta_r$ | $i_a^*$ | $i_b^*$ | $i_c^*$ |
|---|---|---|---|
| 0-160 | $i_{ref}$ | -$i_{ref}$ | 0 |
| 60-120 | $i_{ref}$ | 0 | -$i_{ref}$ |
| 120-180 | 0 | $i_{ref}$ | -$i_{ref}$ |
| 180-240 | -$i_{ref}$ | $i_{ref}$ | 0 |
| 240-300 | -$i_{ref}$ | 0 | $i_{ref}$ |
| 300-360 | 0 | -$i_{ref}$ | $i_{ref}$ |

**Table. 2:** Reference currents for forward motoring and reverse braking

| h1 h2 h3 | $I_a^{ref}$ | $I_b^{ref}$ | $I_c^{ref}$ |
|---|---|---|---|
| 1 0 1 | 0 | I* | -I* |
| 0 0 1 | I* | 0 | -I* |
| 0 1 1 | I* | -I* | 0 |
| 0 1 0 | 0 | -I* | I* |
| 1 1 0 | -I* | 0 | I* |
| 1 0 0 | -I* | I* | 0 |

**Table. 3:** Reference currents for reverse motoring and forward braking

| h1 h2 h3 | $I_a^{ref}$ | $I_b^{ref}$ | $I_c^{ref}$ |
|---|---|---|---|
| 1 0 1 | 0 | I* | -I* |
| 0 0 1 | I* | 0 | -I* |
| 0 1 1 | I* | -I* | 0 |
| 0 1 0 | 0 | -I* | I* |
| 1 1 0 | -I* | 0 | I* |
| 1 0 0 | -I* | I* | 0 |

### *4.2 Hysteresis current controller*

The inverter's switching signals are partially generated by the hysteresis current controller. Hysteresis band PWM is essentially a kind of instantaneous Feedback Current Control (FFC) in which the real current follows the command current inside the hysteresis band. The hysteresis band PWM operation mechanism for half bridge inverters is illustrated in Fig. 5. A sine reference current is produced by the control circuit and then compared to the real phase current wave.

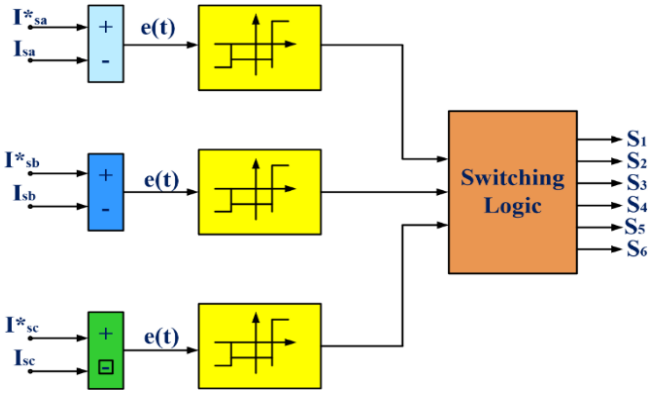


**Fig. 5:** The structure of PWM current controller

The upper switch is turned off and the lower switch is turned on when the current exceeds the upper band limit. The control of the other phase begins when the current exceeds the lower band limit, at which point the upper switch is turned on and the lower switch is turned off. The switching logic is formulated as given below.

If $i_a < (i_a^* - h_b)$ Switch 1 ON and Switch 4 OFF, $S_A = 1$
If $i_a < (i_a^* + h_b)$ Switch 1 ON and Switch 4 OFF, $S_A = 0$
If $i_b < (i_b^* - h_b)$ Switch 3 ON and Switch 6 OFF, $S_A = 1$
If $i_b < (i_b^* + h_b)$ Switch 3 ON and Switch 6 OFF, $S_A = 0$
If $i_c < (i_c^* - h_b)$ Switch 5 ON and Switch 2 OFF, $S_A = 1$
If $i_c < (i_c^* + h_b)$ Switch 5 ON and Switch 2 OFF, $S_A = 0$

In this case, the inverter's output voltage under the a fore mentioned switching conditions is presented below, with $h_b$ representing the hysteresis band surrounding the reference currents for the three phases.

$$v_a = \frac{1}{3}[2S_A - S_B - S_C]$$

$$v_b = \frac{1}{3}[-S_A + 2S_B - S_C]$$

$$v_c = \frac{1}{3}[-S_A - S_B + 2S_C]$$

### *4.3 Modelling of Back EMF using Rotor Position*

From this, the phase back EMF's may be stated as trapezoidal in nature and the function of the speed $\omega_m$ and rotor position angle $\theta_r$ in the PMBLDC motor.

$$\begin{bmatrix} e_a \\ e_b \\ e_c \end{bmatrix} = \omega_m \lambda_m \begin{bmatrix} f_{as}(\theta_r) \\ f_{bs}(\theta_r) \\ f_{cs}(\theta_r) \end{bmatrix}$$

The back emf functions mathematical model as,

$$f_{as}(\theta_r) = \begin{cases} \theta_r \frac{6}{\pi}, & 0 \le \theta_r < \frac{\pi}{6} \\ 1, & \frac{\pi}{6} \le \theta_r < \frac{5\pi}{6} \\ (\pi - \theta_r)\frac{6}{\pi}, & \frac{5\pi}{6} \le \theta_r < \frac{7\pi}{6} \\ -1, & \frac{7\pi}{6} \le \theta_r < \frac{11\pi}{6} \\ (\theta_r - 2\pi)\frac{6}{\pi}, & \frac{11\pi}{6} \le \theta_r < 2\pi \end{cases}$$

$$f_{bs}(\theta_r) = \begin{cases} -1, & 0 \le \theta_r < \frac{\pi}{2} \\ (-\frac{2\pi}{3} + \theta_r)\frac{6}{\pi}, & \frac{\pi}{2} \le \theta_r < \frac{5\pi}{6} \\ 1, & \frac{5\pi}{6} \le \theta_r < \frac{3\pi}{2} \\ (-\frac{5\pi}{3} + \theta_r)\frac{6}{\pi}, & \frac{3\pi}{6} \le \theta_r < \frac{11\pi}{6} \end{cases}$$

$$f_{cs}(\theta_r) = \begin{cases} -1, & \frac{11\pi}{6} \le \theta_r < 2\pi \\ 1, & 0 \le \theta_r < \frac{\pi}{6} \\ \left(\frac{\pi}{3} - \theta_r\right)\frac{6}{\pi}, & \frac{\pi}{6} \le \theta_r < \frac{\pi}{2} \\ -1, & \frac{\pi}{2} \le \theta_r < \frac{7\pi}{2} \\ \left(-\frac{4\pi}{3} + \theta_r\right)\frac{6}{\pi}, & \frac{7\pi}{2} \le \theta_r < \frac{3\pi}{2} \\ 1, & \frac{3\pi}{2} \le \theta_r < 2\pi \end{cases}$$

**Table. 4:** Back EMF modelled as a function of rotor angle

| Theta_elec | $F_a(\theta_r)$ | $F_b(\theta_r)$ | $F_c(\theta_r)$ |
|---|---|---|---|
| $0^0$ - $60^0$ | $\frac{6\theta_r}{\pi} - 1$ | +1 | -1 |
| $60^0$ - $120^0$ | +1 | $3 - \frac{6\theta_r}{\pi}$ | -1 |
| $120^0$ - $180^0$ | +1 | -1 | $\frac{6\theta_r}{\pi} - 5$ |
| $180^0$ - $240^0$ | $7 - \frac{6\theta_r}{\pi}$ | -1 | +1 |
| $240^0$ - $300^0$ | -1 | $\frac{6\theta_r}{\pi} - 9$ | +1 |
| $300^0$ - $360^0$ | -1 | +1 | $11 - \frac{6\theta_r}{\pi}$ |

### *4.4 Closed loop controller*

Three phase MOSFET-based inverter feeds the BLDC motor. To preserve the current constant during the $60^0$ interval of one electrical revolution of the motor, the PWM gating signals for firing the power semiconductor devices in the inverter are pumped from a hysteresis current controller [4]. Table. 4, and Table. 5, represents the back EMF and hall sensors as a function of rotor angle.

**Table. 5:** Hall Sensors simulated as a function of rotor angle

| Theta_elec | $h_1$ $h_2$ $h_3$ |
|---|---|
| $0^0$ - $60^0$ | 1 0 1 |
| $60^0$ - $120^0$ | 0 0 1 |
| $120^0$ - $180^0$ | 0 1 1 |
| $180^0$ - $240^0$ | 0 1 0 |
| $240^0$ - $300^0$ | 1 1 0 |
| $300^0$ - $360^0$ | 1 0 0 |

Specifically, it controls the real current in the hysteresis band surrounding the reference currents. A reference current generator is used to generate the reference currents, and its operation is dependent on the operating mode, which is considered steady state. A quasi square wave pattern characterises the reference currents. As they are developed in phase with the back emf when in motoring mode, they are developed in opposite phases when in braking mode. In order to determine the reference current, one must know the reference torque. Restricting the PI controller's output yields the reference torque. The reference torque is generated by the limiter after the PI controller processes the speed error signal, which is the difference between the reference speed and the actual speed. In order to reduce tracking errors relative to the reference speed, the speed controller receives the sensed actual speed and processes it accordingly. As a result, the control drive system is a closed loop.

## 5. Simulation Results and Discussion

Given the non-linear nature of the model equations, the Runge-Kutta numerical approach is iterated in MATLAB/SIMULINK. The motor performance has been simulated and examined under the following circumstances.

- A comparative analysis of the motor response at various speeds under abrupt load is conducted.
- The dynamics of starting and no-load are studied.
- A relative analysis of various loads applied abruptly at a specific fixed speed.
- The motor's dynamics when the rotor is blocked, for sporadic loads.
- The BLDC motor operates in four quadrants.

### *5.1 Four Quadrant Operation*

Fig. 6, to helps to analyse the initial current draw, stability, and amplitude. These parameters are crucial for evaluating the motor's behaviour during startup and its response to no-load conditions.

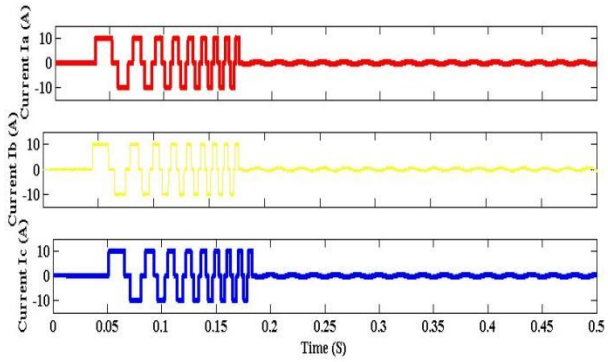


**Fig. 6:** Current waveforms in each phase of the motor during starting and no-load conditions.

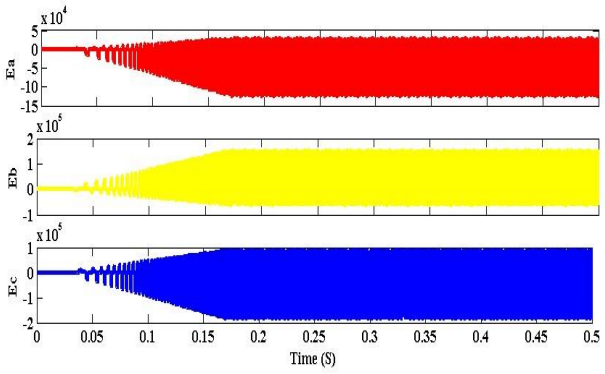


**Fig. 7:** Back EMF waveforms for each motor phase.

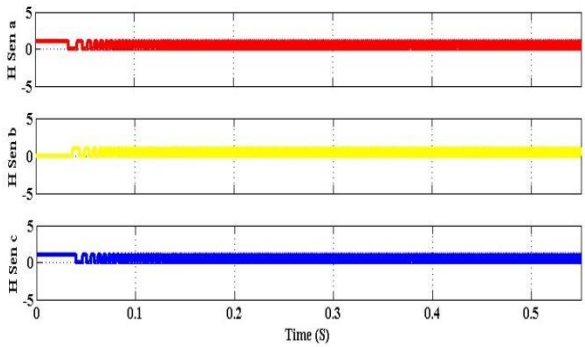


**Fig. 8:** Provides phase-specific outputs from the Hall sensors.

To test the motor's synchronization, efficiency, and commutation system's proper operation, one uses back EMF, which is proportional to the rotor speed this will emphasis in Fig. 7. Fig. 8, gives outputs are essential for detecting the rotor's position and ensuring accurate commutation, which is key to smooth motor operation.

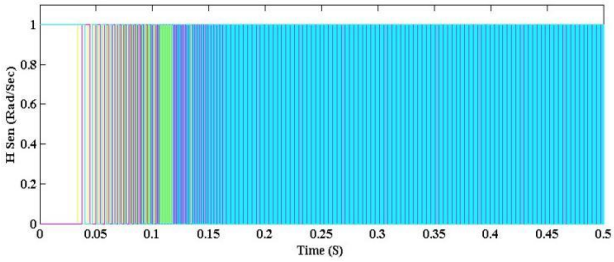


**Fig. 9:** Combines the outputs from all phases to show the overall Hall sensor waveforms.

This Fig. 9, helps in validating the sequence and timing of the Hall sensors' signals, ensuring proper motor operation.

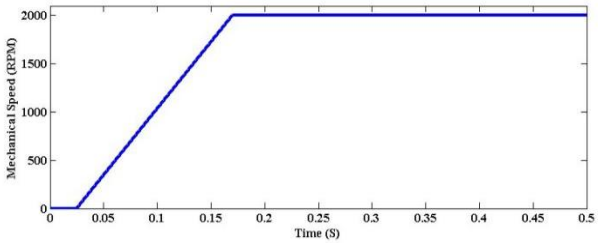


**Fig. 10:** Represents the mechanical speed of motor under starting and zero-load conditions.

Without a load, the speed curve shows how the motor reaches its nominal speed and stays there will shown in Fig. 10.

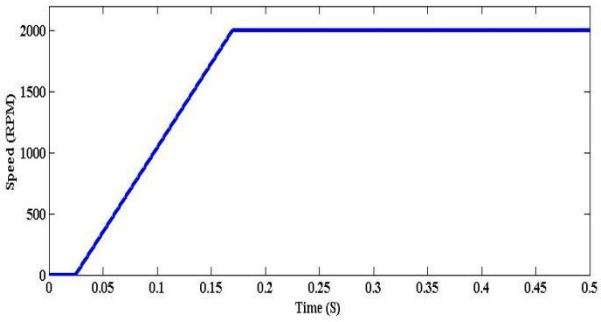


**Fig. 11:** Depicts the variation of motor speed over time.

Fig. 11, shows the starting motor's transient response and steady-state operation time, it is helpful to examine this figure.

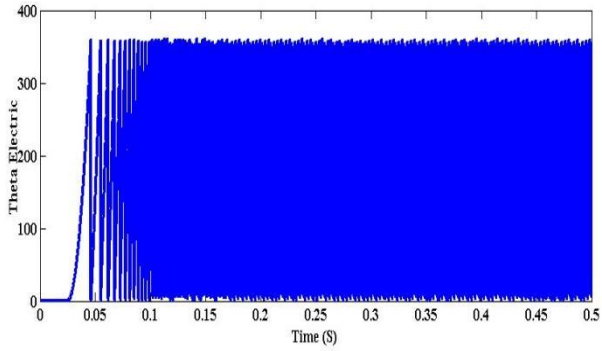


**Fig. 12:** Highlights the relationship between time and rotor position in terms of electric radians.

This Fig. 12, is useful for evaluating rotor phase alignment, ensuring proper synchronization during operation

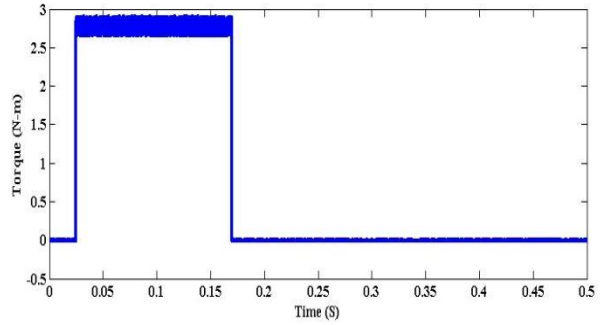


**Fig. 13:** Illustrates how the motor torque varies over time during starting and no-load operation.

This Fig. 13, provides insights into the torque profile, highlighting transient behaviours and stability during no load conditions

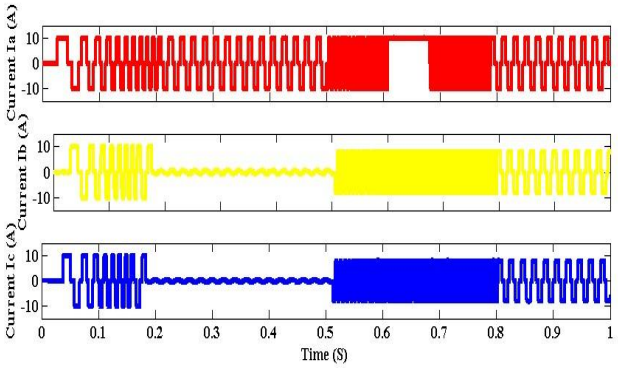


**Fig. 14:** Displays the current waveforms in each phase when the motor operates in reverse.

### *5.2 Reverse Direction*

Fig. 14, highlights the symmetry and transient behaviour of phase currents during the transition to reverse motion, ensuring consistent current regulation.

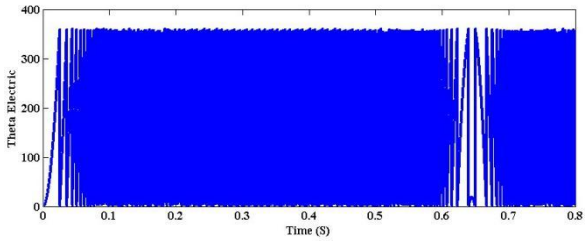


**Fig. 15:** Shows the variation of rotor position (in electric radians) with respect to time during reverse operation.

Fig. 15, helps evaluate the rotor's synchronization and phase alignment during the reversal process

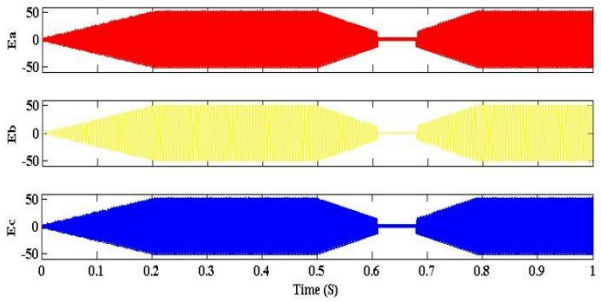


**Fig. 16:** Depicts the back EMF waveforms for individual phases while the motor runs in reverse.

Back EMF is critical for assessing the efficiency of the motor and ensuring proper commutation during reverse operation, as shown in Fig. 16.

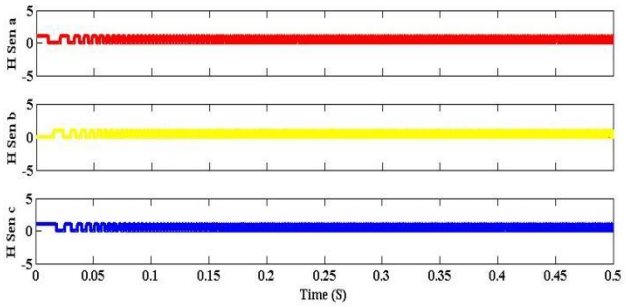


**Fig. 17:** Shows the output signals from the Hall sensors for each phase during reverse direction operation.

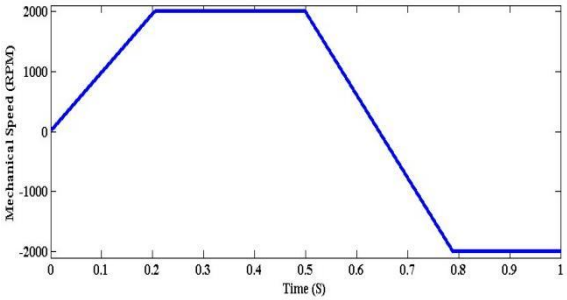


**Fig. 18:** Represents the motor's mechanical speed as it operates in reverse.

Fig. 17, ensures that the Hall sensors provide accurate rotor position feedback, critical for reversing direction without misalignment. Fig. 18, provides insights into how quickly and smoothly the motor transitions to and stabilizes at the desired speed in reverse motion.

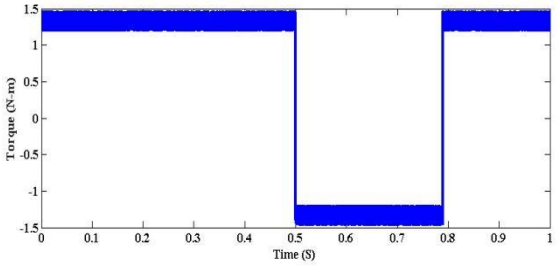


**Fig. 19:** Illustrates the motor's torque variation over time during reverse operation.

This Fig. 19, helps in analysing the torque stability and transient behaviour when the motor changes direction.

### *5.3 Loaded Condition*

Fig. 20, helps analyse how the load affects current stability and magnitude, crucial for evaluating the motor's ability to handle varying load conditions.

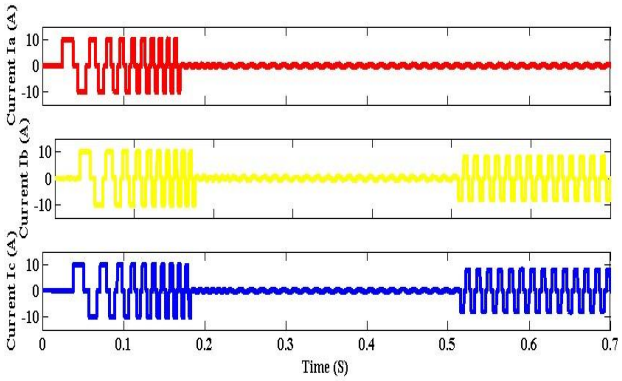


**Fig. 20:** Displays the current waveforms in individual motor phases when the motor operates under a load.

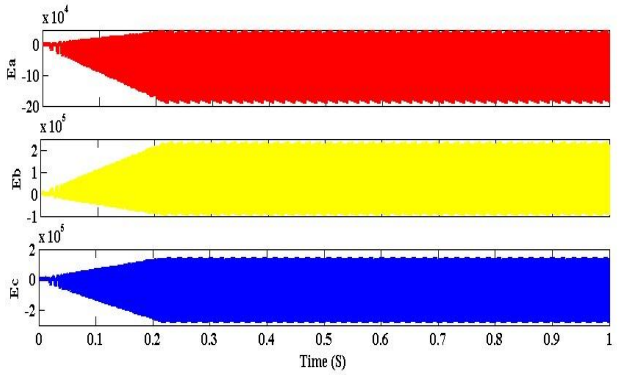


**Fig. 21:** Shows the back EMF waveforms for each phase when the motor is under load.

Back EMF indicates the efficiency of the motor under load and helps in assessing the impact of loading on phase voltage, as shown in Fig. 21.

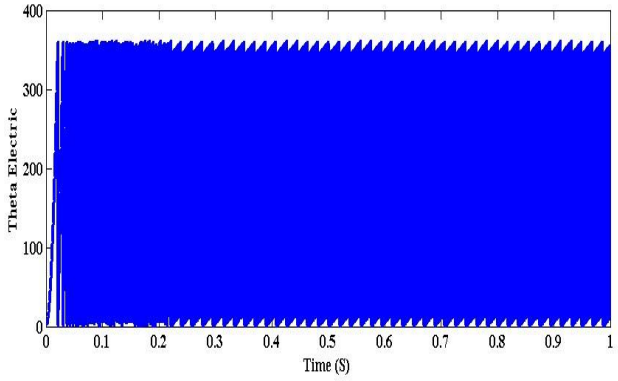


**Fig. 22:** Depicts the rotor's electrical angle in terms of electric radians during loaded operation.

Fig. 22, highlights the rotor's alignment and stability under loaded conditions, critical for proper commutation and efficiency.

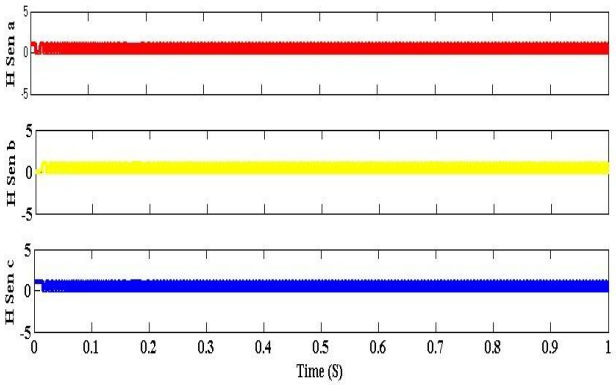


**Fig. 23:** Displays the outputs from Hall sensors for individual phases under loaded conditions.

Fig. 23, helps ensure the hall sensors provide accurate rotor position feedback, even when the motor experiences mechanical stress due to loading.

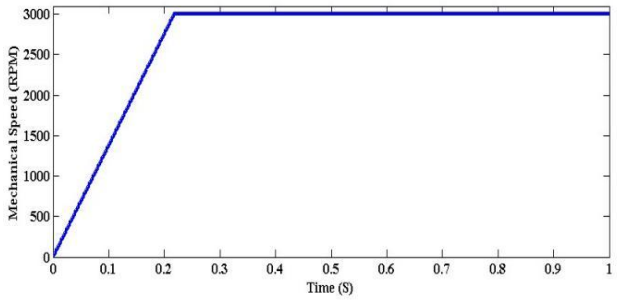


**Fig. 24:** Represents the motor's mechanical speed under loaded conditions.

Fig. 24, evaluates how the motor maintains or adjusts its speed when subjected to load, an essential parameter for performance assessment

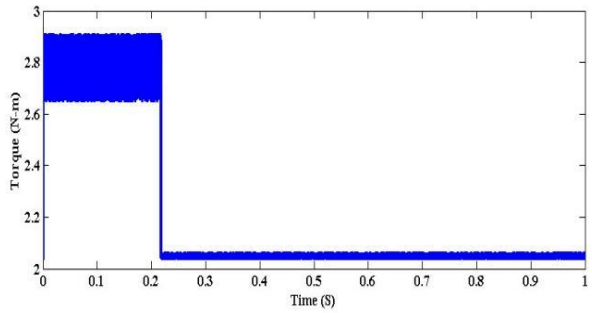


**Fig. 25:** Illustrates the torque response of the motor over time while operating under load.

Fig. 25, shows how the motor generates and stabilizes torque under applied loads, helping in understanding torque consistency and motor performance.

### *5.4 Variable Loaded Condition*

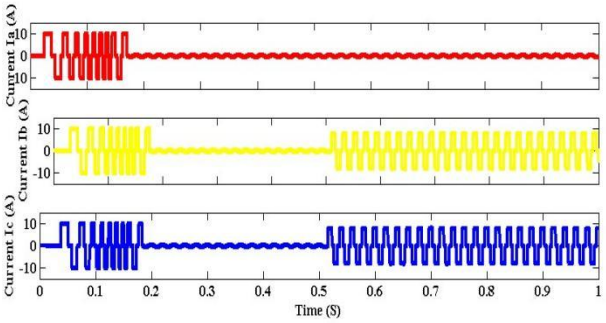


**Fig. 26:** Displays the current waveforms in the motor's phases under varying load levels.

Fig. 26, highlights how the phase currents respond to different load magnitudes, providing insights into the motor's adaptability and current regulation capabilities.

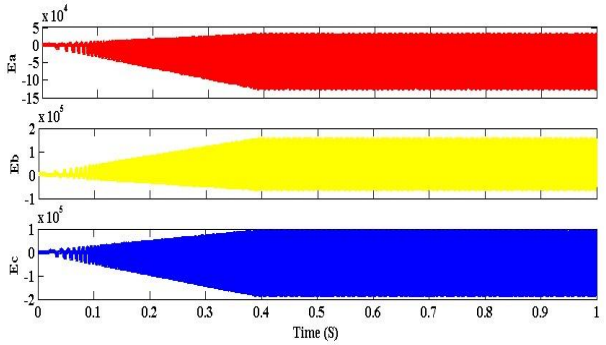


**Fig. 27:** Shows the back EMF waveforms for each phase as the load on the motor changes

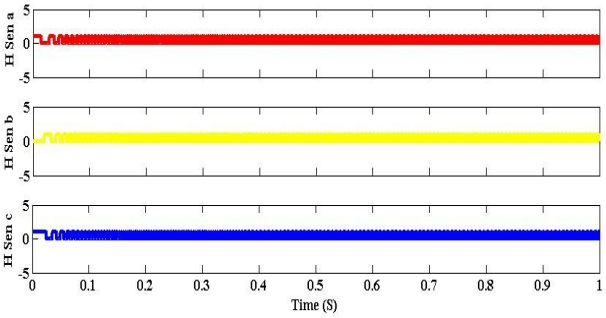


**Fig. 28:** Depicts the hall sensor outputs for individual phases under varying load levels.

Fig. 27, examines how varying loads affect the motor's back EMF, offering a measure of efficiency and stability under dynamic load conditions. Fig. 28, ensures that the hall sensors provide consistent and accurate feedback for rotor position, even as the load changes.

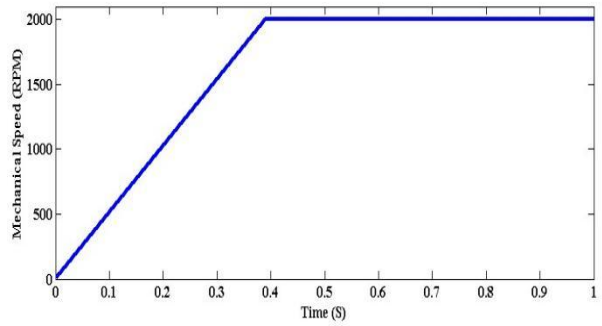


**Fig. 29:** Represents the motor's speed response under varying load levels.

Fig. 29, analyses how the motor adapts its speed to maintain performance as the load fluctuates, a key indicator of system stability. Fig. 30, evaluates the rotor's alignment and commutation precision as the load changes, critical for smooth motor operation.

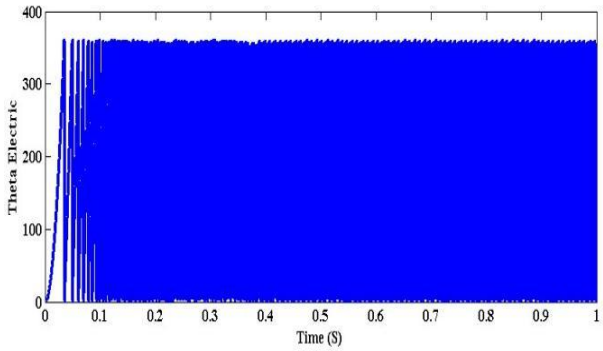


**Fig. 30:** Shows the rotor angle in electric radians under different load conditions.

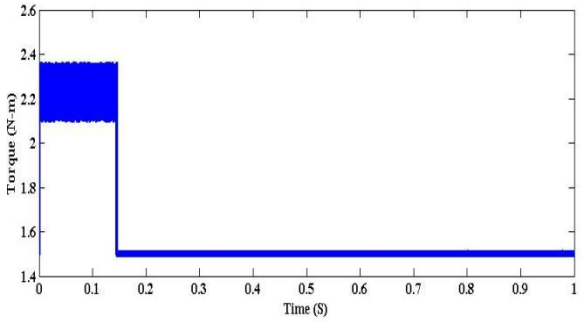


**Fig. 31:** Illustrates how the motor's torque varies over time when subjected to different loads.

Fig. 31, provides insights into the motor's torque stability and capability to handle dynamic load changes effectively.

### *5.5 Novelty and contribution*

Table. 6, emphasizes the comparison between the proposed and existing technologies. Specific Refinements or focus areas are as follows,

- ***Energy Efficiency:*** The proposed technique shows a focus on regenerative braking and energy conservation, making it suitable for energy critical applications like electric vehicles. Advanced controllers like TID and ADRC also shine here.
- ***Torque Ripple Reduction:*** PWM and hysteresis control in the proposed model offer effective ripple management. However, ANFIS and ADRC outperform slightly due to advanced real-time optimizations.

**Table. 6:** Comparison table: proposed vs. existing techniques for BLDC motor control

| Aspect | Proposed Technique | PI/PID Controllers | Fuzzy Logic Controllers | ANFIS (with PSO) | TID Controllers | Second-Order ADRC |
|---|---|---|---|---|---|---|
| **Control Methodology** | Closed-loop with hysteresis current control | Linear control, fixed gains | Rule-based, adaptive to changes | Hybrid (fuzzy + neural network), PSO optimized | Integral-derivative with enhanced stability | Active disturbance rejection with real-time adaptability |
| **Transient Response** | Fast and stable | Moderate, prone to overshoot | Faster than PI/PID, minimal overshoot | Superior to fuzzy logic, optimized settling | Very fast with minimal overshoot | Comparable to TID, robust in transient conditions |
| **Robustness to Load Changes** | High, supports four-quadrant operation | Low, sensitivity to load disturbances | High, adaptable to varying loads | Very high due to PSO optimization | High, maintains stability under varying loads | Very high, excellent disturbance rejection |
| **Energy Efficiency** | Regenerative braking and optimized speed control | Moderate, no regenerative features | High, supports energy-saving features | High, particularly in EV applications | High, optimized for minimal energy loss | Very high, compensates for power losses |
| **Torque Ripple Management** | Effective using PWM and | Poor, limited by fixed control | Good, enhanced by | Excellent, PSO minimizes | Good, improves | Excellent, ensures smooth operation |

| | hysteresis control | strategy | adaptive rules | torque ripple | torque stability | |
|---|---|---|---|---|---|---|
| **Implementation Complexity** | Moderate, simulation-driven optimization | Low, easy to implement | Moderate, requires expertise in fuzzy logic | High, involves PSO and ANFIS hybridization | High, advanced tuning of parameters required | High, requires in-depth tuning and real-time feedback |
| **Applicability** | Broad, suited for industrial and EV applications | Basic, effective for simple systems | Versatile, suitable for various applications | Targeted, ideal for high-performance systems | Broad, excellent for EVs and robotics | High, suitable for precision applications |
| **Sensor Requirements** | Hall sensors | Hall sensors | Hall or sensor less setups | Sensor less with advanced estimation techniques | Sensors or hybrid approaches | Advanced sensing or estimation required |
| **Cost-Effectiveness** | Moderate, balances performance and cost | High, minimal hardware/software cost | Moderate, needs specialized components | Low, high computational and hardware needs | Moderate, good for high-efficiency systems | Low, advanced hardware/software required |
| **Scalability** | Easily scalable to different applications | Simple scaling for similar systems | Moderate, rule set needs adaptation | Moderate to high, scalable with optimization | Moderate, requires re-tuning for scaling | High, adaptable to various configurations |

**Table. 7:** Summarizing the proposed technique versus existing techniques for BLDC motor control

| Feature/Aspect | Proposed Technique (MATLAB/SIMULINK Model) | Existing Techniques |
|---|---|---|
| Control Approach | Closed-loop PI-based with hysteresis current controller | PI, PID, Fuzzy Logic, ANFIS, Second-Order ADRC, TID |
| Dynamic Performance | High, with effective current and speed control | Moderate to high, depending on the technique (e.g., ANFIS provides better transient response) |
| Robustness to Disturbances | Enhanced due to closed loop design and four-quadrant operation | Limited for PI/PID; Higher for fuzzy logic and ADRC |
| Adaptability to Nonlinearities | Improved handling through hysteresis based control | Poor for linear controllers (PI, PID); good for fuzzy logic and ANFIS |
| Implementation Complexity | Moderate, requires precise parameter tuning | Varies: Low for PI/PID, high for ANFIS, ADRC, and TID |
| Energy Efficiency | High, with regenerative braking and efficient torque control | High for fuzzy logic and advanced controllers like TID |
| Sensor Requirements | Hall sensors for rotor position | Varies: sensor less techniques (e.g., ANFIS+PSO); Hall sensors in simpler systems |
| Application Suitability | Suitable for industrial and EV applications | Widely varied, with specific focus areas like dental motors, EVs, robotics |
| Response Time | Fast transient response | Slower for conventional PI/PID; Faster for ANFIS and ADRC |
| Torque Ripple Reduction | Effective through PWM modulation and hysteresis control | Advanced methods like PWM-PWM and ADRC offer better performance |

- ***Cost-Effectiveness**:* The proposed system offers a balance, but conventional PI/PID controllers are far cheaper and easier to implement in simpler applications.
- ***Robustness and Adaptability**:* The proposed method's closed-loop hysteresis design provides robustness but falls behind hybrid models like ANFIS+PSO and ADRC in handling extreme nonlinearities or high-speed dynamics.

Table. 7, encapsulates the comparative performance of the proposed MATLAB/Simulink model versus other techniques discussed

## 6. Conclusion

This article presents how to use MATLAB/Simulink to build, simulate, and analyse

dynamically a BLDC motor drive system, with an emphasis on four-quadrant operation in a variety of environments. The proposed model effectively integrates closed loop PI control with hysteresis current control, ensuring improved speed and torque regulation. Simulation results validate the model's ability to achieve fast transient response, robust performance against load variations, and efficient energy utilization through regenerative braking. Compared to traditional PI and PID controllers, the proposed method offers superior adaptability to nonlinearities and load disturbances. While fuzzy logic and hybrid techniques like ANFIS provide advanced capabilities, the proposed model strikes an optimal balance between implementation complexity, cost, and performance, making it a viable solution for a broad range of industrial and electric vehicle applications. In order to improve the efficiency and robustness of BLDC motor drives, the results highlight the significance of using advanced control schemes and optimisation methods. Future research could explore hardware implementation and further optimization, such as incorporating AI - based adaptive controllers, to enhance system performance in real world applications.

## Conflict of Interest

The authors declared "No conflict of interest".

## Funding

This research received no external funding.

## Data Availability Statement

Data sharing is not applicable to this article as no datasets were generated or analyzed.

## CRediT authorship contribution statement

Both authors contributed to this manuscript equally. Both authors have read and agreed to the published version of the manuscript.

## References

[1] O. M. Neda, "Enhancing Performance of BLDC: An Improved Fast Terminal Slide Mode Control for BLDC Motor Speed Control", *Franklin Open*, Vol. 14, art. no. 100510, 2026. https://doi.org/10.1016/j.fraope.2026.100510

[2] M. Megrini, A. Gaga, and Y. Mehdaoui, "Processor in the loop implementation of artificial neural network controller for BLDC motor speed control", *Results in Engineering*, Vol. 23, art. no. 102422, 2024. https://doi.org/10.1016/j.rineng.2024.102422

[3] N. Hemalatha, S. Venkatesan, R. Kannan, S. Kannan, A. Bhuvanesh, and A. S. Kamaraja, "Sensorless speed and position control of permanent magnet BLDC motor using particle swarm optimization and ANFIS", *Measurement: Sensors*, Vol. 31, art. no. 100960, 2024. https://doi.org/10.1016/j.measen.2023.100960

[4] M. Subbarao, K. Dasari, S. S. Duvvuri, K. R. K. V. Prasad, B. K. Narendra, and V. B. Murali Krishna, "Design, control and performance comparison of PI and ANFIS controllers for BLDC motor driven electric vehicles", *Measurement: Sensors*, Vol. 31, art. no. 101001, 2024. https://doi.org/10.1016/j.measen.2023.101001

[5] S. N. Tripathy, S. Kundu, A. Pradhan, and P. Samal, "Optimal design of a BLDC motor using African vulture optimization algorithm", *e-Prime - Advances Electrical Engineering Electronics and Energy*, Vol. 7, art. no. 100499, 2024. https://doi.org/10.1016/j.prime.2024.100499

[6] G. Kaczmarczyk, M. Malarczyk and M. Kaminski, "Stable Rules Definition for Fuzzy TS Speed Controller Implemented for BLDC Motor", *Applied Sciences*, Vol. 14, No. 3, 2024. https://doi.org/10.3390/app14030982

[7] G. Park and J. S. Lim, "A Study on Ways to Expand the Speed Operation Range of Dental Laboratory Handpiece Motors Using Low-Cost Hall Sensors", *Electronics*, Vol. 13, No. 21, 2024. https://doi.org/10.3390/electronics13214259

[8] K. Kroics and A. Bumanis, "BLDC Motor Speed Control with Digital Adaptive PID-Fuzzy controller and Reduced Harmonic Content", *Energies*, Vol. 17, No. 6, art. no. 1311, 2024. https://doi.org/10.3390/en17061311

[9] K. Sayed, H. H. El-Zohri, A. Ahmed, and M. Khamies, "Application of Tilt Integral Derivative for Efficient Speed Control and Operation of

BLDC Motor Drive for Electric Vehicles", *Fractal and Fractional*, Vol. 8, No. 1, 2024. https://doi.org/10.3390/fractalfract8010061

[10] P. Zhang, Z. Shi, B. Yu, and H. Qi, "Research on the Control Method of a Brushless DC Motor Based on Second Order Active Disturbance Rejection Control", *Machines*, Vol. 12, No. 4, 2024. https://doi.org/10.3390/machines12040244

[11] G. H. Raeisi Hasanhendoei, E. Afjei, M. Naseri, and S. Azad, "Automatic and real time phase advancing in BLDC motor by employing an electronic governor for a desired speed-torque/angle profile," *e-Prime Advances Electrical Engineering Electronics Energy*, Vol. 4, art. no. 100111, 2023. https://doi.org/10.1016/j.prime.2023.100111

[12] G. Yao, J. Feng, G. Wang, and S. Han, "BLDC Motors Sensorless Control Based on MLP Topology Neural Network", *Energies*, Vol. 16, No. 10, 2023. https://doi.org/10.3390/en16104027

[13] B. Surakasi, R. Satish, B. Pydi, H. Kotb, M. Shouran, and B. Abdul Samad, "A Novel Methodology to Enhance the Smooth Running of the PM BLDC Motor Drive Using PWM-PWM Logic and Advance Angle Method", *Machines*, Vol. 11, No. 1, 2022. https://doi.org/10.3390/machines11010041

[14] B. Mahesh Kumar and R. Babu Ashok, "Speed control of brushless DC motor in four quadrant operation using DSP", *International Journal of Applied Engineering Research*, Vol. 10, No. 7, pp. 17919–17931, 2015.

[15] B. Ananthababu, C. Ganesh and C. V. Pavithra, "Fuzzy based speed control of BLDC motor with bidirectional DC-DC converter", *2016 Online International Conference on Green Engineering and Technologies (IC-GET)*, pp. 1 - 6, 2016.

[16] R. J. Masood, D. B. Wang, Z. A. Ali, and B. Khan, "DDC control techniques for three-phase BLDC motor position control", *Algorithms*, Vol. 10, No. 4, 2017. https://doi.org/10.3390/a10040110

[17] M. Gopinath, T. Yuvaraja, and S. Jeykumar, "Implementation of Four Quadrant Operation of BLDC Motor Using Model Predictive Controller", *Materials Today Proceedings*, Vol. 5, No. 1, pp. 1666 – 1672, 2018. https://doi.org/10.1016/j.matpr.2017.11.261

[18] D. Potnuru, K. A. Mary and Ch. Saibabu, "Design and implementation methodology for rapid control prototyping of closed loop speed control for BLDC motor", *Journal of Electrical Systems Information Technology*, Vol. 5, No. 1, pp. 99 – 111, 2018. https://doi.org/10.1016/j.jesit.2016.12.005

[19] S. Tiwari and S. Rajendran, "Four Quadrant Operation and Control of Three Phase BLDC Motor for Electric Vehicles," *2019 IEEE PES GTD Grand International Conference Exposition Asia, (GTD Asia)*, pp. 577–582, 2019. https://doi.org/10.1109/GTDAsia.2019.8715878

[20] A. D. G. Jegha, M. S. P. Subathra, N. M. Kumar, U. Subramaniam, and S. Padmanaban, "A high gain DC-DC converter with grey wolf optimizer based MPPT algorithm for PV fed BLDC motor drive", *Applied Sciences*, Vol. 10, No. 8, 2020. https://doi.org/10.3390/app10082797

[21] A. K. Singh and S. Pattnaik, "Matrix Converter Operated Hysteresis Current Controlled BLDC Motor Drive for Efficient Speed Control and Improved Power Quality", *Procedia Computer Science*, Vol. 167, pp. 541–550, 2020. https://doi.org/10.1016/j.procs.2020.03.314

[22] E. B. Kashani and A. H. Niasar, "Reduction of torque ripple in an electrolytic capacitor-less BLDC motor drive by simultaneous speed and torque control method", *Ain Shams Engineering Journal*, Vol. 12, No. 4, pp. 3703–3709, 2021. https://doi.org/10.1016/j.asej.2020.12.021

[23] K. Smółka, A. F. Nowacka, and S. Wiak, "Comparison of the Design of 3-Pole BLDC Actuators/Motors with a Rotor Based on a Single Permanent Magnet", *Sensors*, Vol. 22, No. 10, 2022. https://doi.org/10.3390/s22103759



***